The Astrophysical Journal Letters, 880:L28 (7pp), 2019 August 1 https://doi.org/10.3847/2041-8213/ab30ca

Possible Early Linear Acceleration of Proto-neutron Stars via Asymmetric Neutrino Emission in Core-collapse Supernovae

Hiroki Nagakura[1], Kohsuke Sumiyoshi[2], and Shoichi Yamada[3,4]
[1] Department of Astrophysical Sciences, Princeton University, Princeton, NJ 08544, USA; hirokin@astro.princeton.edu
[2] Numazu College of Technology, Ooka 3600, Numazu, Shizuoka 410-8501, Japan
[3] Advanced Research Institute for Science & Engineering, Waseda University, 3-4-1 Okubo, Shinjuku, Tokyo 169-8555, Japan
[4] Department of Science and Engineering, Waseda University, 3-4-1 Okubo, Shinjuku, Tokyo 169-8555, Japan
Received 2019 March 19; revised 2019 July 1; accepted 2019 July 9; published 2019 July 31

Abstract

In this Letter we present the result of an axisymmetric core-collapse supernovae simulation conducted with appropriate treatments of neutrino transport and proper motions of proto-neutron stars (PNSs), in which a remarkable PNS acceleration is observed in association with asymmetric neutrino emissions 300 ms after bounce. We find that these asymmetric neutrino emissions play important roles in the acceleration of PNSs in this phase. The correlation between the PNS proper motion and the asymmetric ejecta is similar to that in a neutron star (NS) kick of hydrodynamic origin. Both electron-type neutrinos ($\nu_{\rm e}$) and their anti-particles ($\bar{\nu}_{\rm e}$) have a $\sim$10% level of asymmetry between the northern and southern hemispheres, while other heavy-leptonic neutrinos (ν_x) have much a smaller asymmetry of $\sim$1%. The emissions of $\bar{\nu}_{\rm e}$ and ν_x are higher in the hemisphere of stronger shock expansion, whereas the $\nu_{\rm e}$ emission is enhanced in the opposite hemisphere: in total, the neutrinos carry some linear momentum to the hemisphere of the stronger shock expansion. This asymmetry is attributed to the non-spherical distribution of electron-fraction (Y_e) in the envelope of PNS. Although it is similar to lepton-emission self-sustained asymmetry, the Y_e asymmetry seems to be associated with the PNS motion: the latter triggers lateral circular motions in the envelope of PNS by breaking the symmetry of the matter distribution there, which is then sustained by a combination of convection, lateral neutrino diffusion, and matter-pressure gradient. Our findings may have an influence on the current theories on the NS kick mechanism, although long-term simulations are required to assess their impact on later evolution.

Key words: hydrodynamics – neutrinos – radiative transfer – supernovae: general

1. Introduction

There is growing evidence that core-collapse supernovae (CCSN) are highly non-spherical phenomena. The role of their asymmetry during the explosion phase is important: for instance, it is well established that multi-dimensional (multi-D) hydrodynamic instabilities are one of the key ingredients that trigger explosion (see recent reviews, e.g., by Foglizzo et al. 2015; Janka et al. 2016; Mirizzi et al. 2016; Müller 2016). As a consequence of non-spherical explosions, the nascent neutron star (NS), which is left behind at the center of the explosion, inevitably receives a kick (see, e.g., a review by Lai 2001 and references therein). This may account for the fast proper motions of pulsars, which typically move at a few hundreds km s^{-1} (Lyne & Lorimer 1994; Arzoumanian et al. 2002; Chatterjee et al. 2005; Hobbs et al. 2005; Faucher-Giguère & Kaspi 2006; Winkler & Petre 2007).

The NS kick mechanism has been one of the primary research subjects in the CCSN community. If it is of hydrodynamic origin, in which case the NS is accelerated by hydrodynamic or gravitational forces (or both) exerted by the asymmetric ejecta, then it should be kicked in the opposite direction to the hemisphere of stronger explosion. Recently, X-ray observations of young CCSN remnants by Holland-Ashford et al. (2017, 2019) and Katsuda et al. (2018) found such a correlation between the kick direction and the asymmetry of ejecta, hence supporting the hydrodynamic mechanism. However, such a correlation is just one of the necessary conditions and cannot be a smoking gun of that particular mechanism, because other mechanisms may generate the same correlation. On the other hand, previous studies suggest that asymmetric neutrino emissions from a proto-neutron star (PNS) are not large enough to accelerate PNSs to a few hundreds km s^{-1} (Scheck et al. 2004, 2006; Nordhaus et al. 2010, 2012; Wongwathanarat et al. 2013; Janka 2017; Gessner & Janka 2018; Müller et al. 2018). Other mechanisms also require rather extreme conditions to produce the large PNS kick that has been observed. Based on these facts, the hydrodynamic origin is currently the most favored mechanism for the NS kick. Note that in this mechanism the NS kick is produced at rather late times, when the stalled shock has been already revived and an explosion has been firmly established.

In this Letter we study the possible initiation of PNS acceleration in an earlier phase based on the result of one of our latest axisymmetric CCSN simulations. This study is motivated by the fact that there has been no CCSN simulation that handles the PNS proper motions and their feedback to both hydrodynamics and neutrino transport fully self-consistently. Note that, although Scheck et al. (2006) also implemented a moving mesh technique to treat PNS proper motions, it was applied to the hydrodynamics and not to the neutrino transport. In addition, they excised the interior of the PNS in their simulations, which is distinctly different to the simulation presented in this Letter. This is hence the first-ever attempt to perform this aspect in Boltzmann neutrino-radiation-hydrodynamic simulations. We find that the self-consistent treatment

turns out to be crucial: indeed, a remarkable PNS motion occurs in association with large asymmetric neutrino emissions.

The CCSN dynamics obtained in our simulation are aligned with the neutrino-heating explosion mechanism, although the computation is not long enough to make a firm conclusion. We did not incorporate magnetic fields, rotations, and non-standard neutrino physics in this simulation; therefore, the result presented in this Letter is distinct from other mechanisms for producing PNS proper motions that advocate asymmetric neutrino emissions (Bisnovatyi-Kogan 1993; Fuller et al. 2003; Kusenko et al. 2008; Sagert & Schaffner-Bielich 2008). Interestingly, although the property of asymmetric neutrino emissions is the same as in lepton-emission self-sustained asymmetry (LESA), the origin may be different from that discussed in Tamborra et al. (2014), Glas et al. (2018), and Powell & Müller (2018). In fact, we find that the non-spherical neutrino emissions are caused by the asymmetry in the electron-fraction (Y_e) distribution in the envelope of PNS, which is in turn associated with the PNS motion.

2. Method and Model

We carry out an axisymmetric simulation of a CCSN, solving Boltzmann equations for multi-species, multi-energy, and multi-angle neutrino transport. The special relativistic effect in neutrino transport is fully taken into account (Nagakura et al. 2014). A moving mesh technique is implemented in order to treat PNS proper motions self-consistently (Nagakura et al. 2017), which is the most important feature of this Letter. The reliability of our code was established by a detailed comparison with a Monte Carlo simulation (Richers et al. 2017). Very recently, we further developed a new treatment of the momentum feedback from neutrino to matter (Nagakura et al. 2019b). In this method, the momentum exchange is calculated with the energy-momentum tensor instead of by the direct integral of the collision term in the diffusion regime, which substantially improved the accuracy of momentum conservation in our simulations.

Most parts of the numerical setup and input physics are the same as those used in Nagakura et al. (2018). We solve radiation-hydrodynamics with Newtonian self-gravity consistently. Note that we recently improved the treatment of nuclear weak interactions, which is meant to be used with the multi-nuclear equation of state (EOS) based on the variational method (Togashi & Takano 2013; Furusawa et al. 2017). We constructed new tables of electron captures by heavy and light nuclei and positron captures by light nuclei, employing the nuclear abundances provided by the EOS (see Nagakura et al. 2019a for more details). We incorporate all of these updates in the simulation.

A $11.2\,M_\odot$ progenitor model by Woosley et al. (2002) is used. The spherical coordinates (r, θ) are meshed with 384 (r) $\times$ 128(θ) grid points covering $0 \leqslant r \leqslant 5000$ km and $0^\circ \leqslant \theta \leqslant 180^\circ$ in the meridian section, respectively. The momentum space for neutrinos with the energy range of $0 \leqslant \varepsilon \leqslant 300$ MeV and the entire solid angle (Ω) is covered with 20(ε) $\times$ 10($\tilde{\theta}$) $\times$ 6($\tilde{\phi}$) grid points, respectively, where $\tilde{\theta}$ and $\tilde{\phi}$ are the zenith and azimuth angles of neutrino momentum. We consider three neutrino species: electron-type neutrinos ν_e, electron-type anti-neutrinos $\bar{\nu}_e$, and all the others collectively denoted by ν_x. The simulation is run up to 300 ms after bounce.

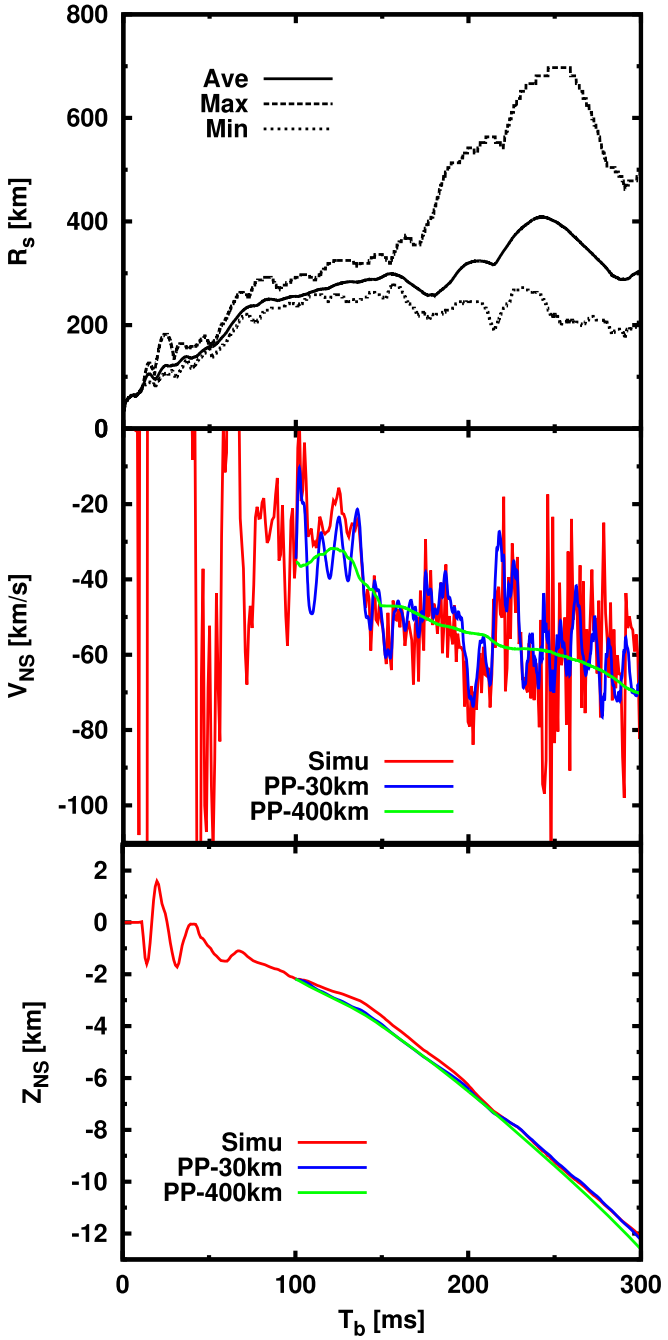

Figure 1. Top panel: time evolutions of the maximum, minimum, and average shock radii. Middle panel: time evolution of the PNS velocity in the simulation (red line). The blue and green lines show the post-processed (PP) results in the PNS kick analysis (see the text for details). Bottom panel: time evolution of the spatial displacement of PNS (red line) in the z direction. The blue and green lines display the results obtained in the post-processing.

3. CCSN Dynamics and PNS Kick

Prompt convection begins at $T_b \sim 10$ ms (T_b denotes the time after bounce) and generates non-spherical fluctuations that will become a seed perturbation for later fluid instabilities in the post-shock flow. The neutrino-driven convection starts to appear at $T_b \sim 100$ ms and triggers a rapid shock expansion in the northern hemisphere at $T_b \sim 180$ ms (see the top panel in Figure 1). Note that we cannot clearly judge at $T_b = 300$ ms (the end of our simulation) whether or not this model leads to explosion (see also Buras et al. 2006; Müller et al. 2012;

Takiwaki et al. 2014; Pajkos et al. 2019), and a longer computation is definitely required for that purpose. Nonetheless, we find a coherent PNS motion clearly up to this point, which may lead to a launch of the NS kick if the model explodes and survives. Because we expect that this proper motion will continue in the subsequent phase of a runaway asymmetric shock expansion, it warrants a detailed analysis.

The red lines in the middle and bottom panels of Figure 1 display the time evolutions of the velocity ($V_{\rm NS}$) and spatial displacement ($Z_{\rm NS}$) of the PNS, respectively.[5] Because the large temporal variations at $T_{\rm b} \lesssim 100$ ms due to the prompt convection are rather random and will not be directly relevant to the PNS acceleration, hereafter we will focus on the later phase $T_{\rm b} > 100$ ms. Although $V_{\rm NS}$ is fluctuating rapidly due to our implementation of the moving mesh technique,[6] it is clear that the PNS receives a linear momentum to the south from $T_{\rm b} \sim 150$ ms. At the end of the simulation, the velocity and the displacement reach $V_{\rm NS} \sim 60\,{\rm km\,s^{-1}}$ and $Z_{\rm NS} \sim 12$ km, respectively, and the PNS is still accelerating in the same direction.

Following common practice, we post-process the result to see what forces dictate the PNS motion. We evaluate the matter acceleration ($a_{\rm tot}$) in the region of $r \leqslant R$, where r denotes the radius measured from the mass center of PNS, which can be written as

$$a_{\rm tot}(R) = a_{\rm m}(R) + a_{\rm p}(R) + a_{\rm g}(R) + a_{\nu}(R), \quad (1)$$

where $a_{\rm m}$, $a_{\rm p}$, $a_{\rm g}$, and a_{ν} represent the contributions from the momentum flux and matter pressure, gravity, and neutrino-matter interactions, respectively. Each term can be expressed as

$$a_{\rm m}(R) \equiv -\frac{R^2\int_{r=R}\rho v_z v^r d\Omega}{M(R)},$$
$$a_{\rm p}(R) \equiv -\frac{R^2\int_{r=R}P\cos\theta d\Omega}{M(R)},$$
$$a_{\rm g}(R) \equiv -\frac{\int_{r\leqslant R}\rho\psi_{,z}dV}{M(R)},$$
$$a_{\nu}(R) \equiv -\frac{\int_{r\leqslant R}G_z dV}{M(R)}, \quad (2)$$

where ρ, v_z, P, ψ, G_z, and V denote the baryon mass density, z-component of fluid velocity, matter pressure, gravitational potential, z-component of momentum transfer from neutrino to matter[7], and spatial volume, respectively. $M(R)$ is the baryon mass in the region ($r \leqslant R$). We display the result in Figure 2, which is obtained by integrating Equations (1) and (2) at three different radii ($R = 30$, 50, and 400 km). Note that the time-integration starts at $T_{\rm b} = 100$ ms in order to remove the contribution from the prompt convection.

At $R = 30$ km (see the top panel of Figure 2), the anisotropies of gravity and matter pressure are the dominant forces, but almost cancel each other out. The neutrino contribution is roughly 10% of them, and the anisotropy in momentum flux is negligible. Note that the blue lines in the middle and bottom panels of Figure 1 are calculated from $a_{\rm tot}$ at $R = 30$ km. We find that the velocities and displacements obtained in the post-process are consistent with the PNS proper motion observed in the simulation.[8] At first glance, the anisotropic matter pressure may look dominant as a driving force of PNS motion (see the phase $T_{\rm b} \gtrsim 150$ ms). However, it is too early to reach this conclusion, as the condition strongly

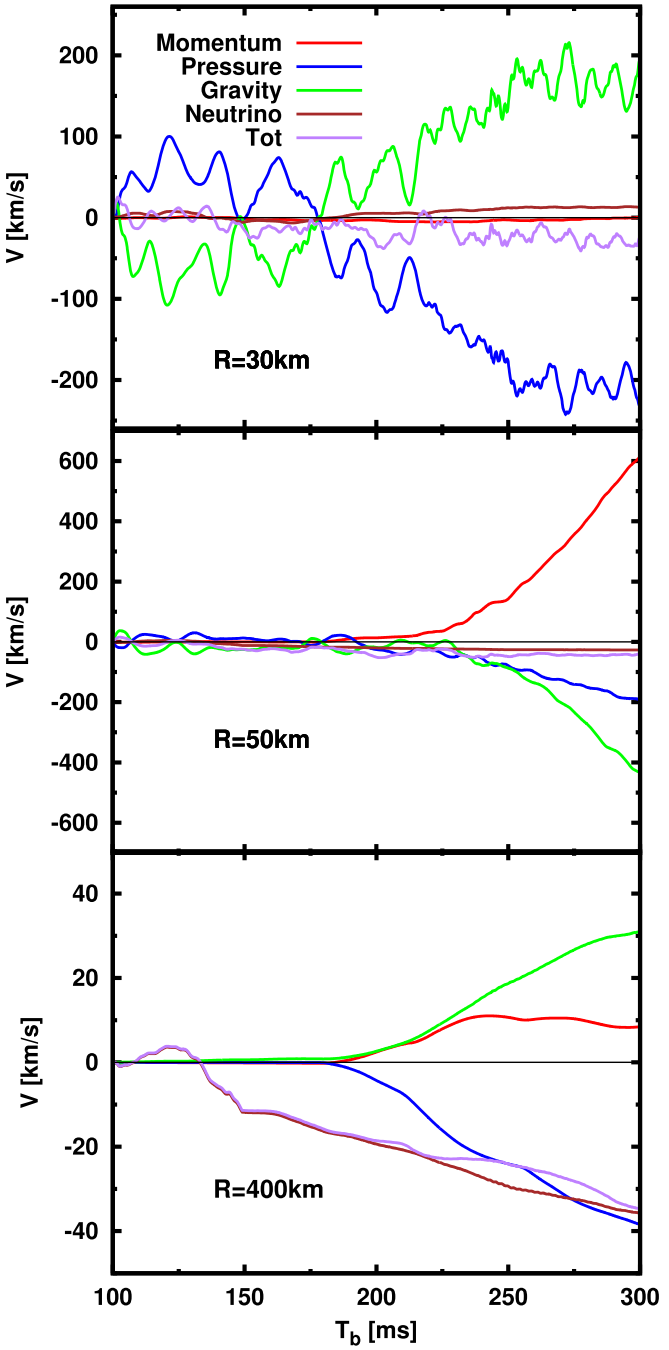

Figure 2. Time evolutions of various contributions to the PNS kick. From the top to bottom panels, we display the results of individual terms in Equations (1) and (2) at $R = 30$, 50, and 400 km, respectively.

[5] The velocity actually corresponds to the shift vector, which is chosen to track approximately the motion of PNS (see Nagakura et al. 2017).

[6] See Nagakura et al. (2017) for more details on the origin of the noise.

[7] The exact form of neutrino-matter interaction can be seen in H. Nagakura et al. (2017, 2019, in preparation).

[8] Note that the initial values of $V_{\rm NS}$ and $Z_{\rm NS}$ for the post-process are derived from the simulation.

depends on the radius. In fact, at $R = 50$ km (in the middle panel of Figure 2), the gravity term changes sign and overwhelms the pressure term. However, the sum of the gravity and pressure contributions is almost canceled by that from the momentum flux. On the other hand, the neutrino contribution, which also has opposite signs at these two radii, is comparable to the total acceleration. This is an indication that neutrinos are not streaming completely freely but are still mildly coupled with matter in the region of $30 \lesssim r \lesssim 50$ km. Because of this strong dependence on radius, it is hard to identify which component is the most dominant player driving the PNS proper motion (see also Nordhaus et al. 2010).

On the other hand, we find another interesting result from the same analysis but applied to a larger radius ($R = 400$ km), which is shown in the bottom panel of Figure 2. The contributions from gravity and hydrodynamic forces become much smaller than those at the smaller radii, and the neutrino contribution overwhelms other ones. This result is not surprising, because all acceleration terms except for the neutrino term tend to zero asymptotically. What is interesting here is that $a_{\rm tot}(R = 400\,{\rm km})$ is comparable with the acceleration of the PNS obtained in the simulation. As a matter of fact, $V_{\rm NS}$ and $Z_{\rm NS}$ calculated in the post-process are roughly consistent with the PNS motion observed in the simulation (see the green lines in the middle and bottom panels of Figure 1). This fact indicates that the role of neutrinos cannot be ignored in the PNS acceleration.

It is important to emphasize that this result is new with regard to CCSN simulations. This is because self-consistent handling of the feedback from PNS proper motions to both hydrodynamics and neutrino transport is indispensable, but this was not realized in previous studies. In fact, most previous simulations have employed some pragmatic prescriptions to either PNS proper motions or neutrino transport (or both), and they may have artificially suppressed the phenomenon. More detailed studies are needed in the future to confirm this.

4. Asymmetric Neutrino Emissions

We now turn our attention to the asymmetric neutrino emission. As shown in the top panel of Figure 3, coherent asymmetric neutrino emissions are clearly seen from $T_{\rm b} \sim 150$ ms, which roughly coincides with the time of the initiation of the asymmetric shock expansion and the PNS acceleration. The $\nu_{\rm e}$ luminosity is stronger in the southern hemisphere (the direction of the PNS motion), whereas the $\bar{\nu}_{\rm e}$ luminosity has the opposite trend (higher in the direction of the stronger shock expansion). Although the asymmetry in ν_x is smaller than in others, it is higher in the northern hemisphere.

Both asymmetries in $\nu_{\rm e}$ and $\bar{\nu}_{\rm e}$ emissions are due to the asymmetric distribution of Y_e around the surface of the PNS (see the bottom panels of Figures 3 and 4). The Y_e in the northern hemisphere is somewhat smaller than in the southern hemisphere: for instance, it is ∼10% smaller than the angle average for $r = 20$ km at $T_{\rm b} \gtrsim 200$ ms. Because the high-Y_e environment produces stronger $\nu_{\rm e}$ and weaker $\bar{\nu}_{\rm e}$ emissions, this is consistent with the trend of the neutrino asymmetry in the simulation. Note that this region is semi-transparent to neutrinos: in fact, $\nu_{\rm e}$ and $\bar{\nu}_{\rm e}$ start to decouple with matter in

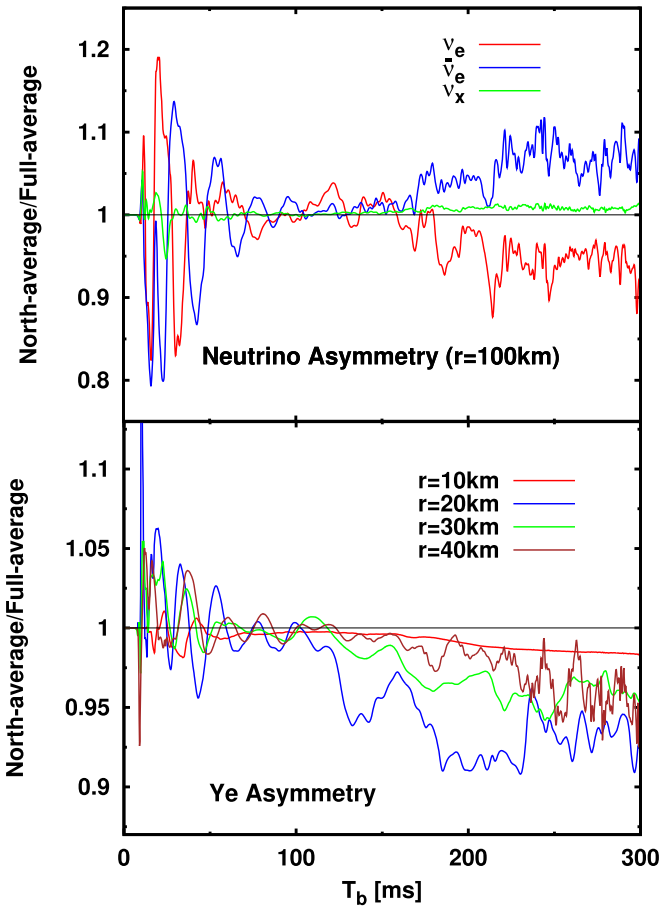

Figure 3. Top panel: time evolutions of the neutrino asymmetry at $r = 100$ km, measured by the ratio of the northern-hemispheric average to the full-spherical average of neutrino luminosity. By definition, it is larger than 1 if the northern hemisphere has a higher luminosity than the southern hemisphere, and vice versa. Bottom panel: the same as the top panel but for Y_e asymmetry. The color represents the results at different radii.

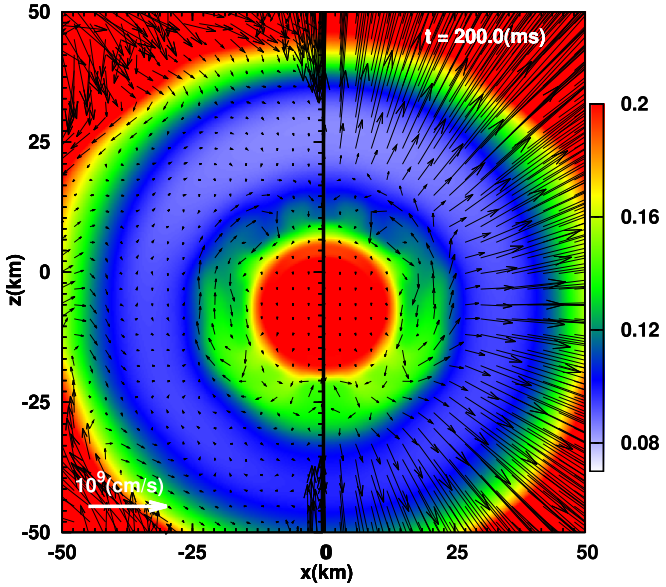

Figure 4. The Y_e distributions in color with the matter velocity vector (left panel) and the energy flux of $\nu_{\rm e}$ measured in the laboratory frame (right panel) normalized by the energy density as vectors at $T_{\rm b} = 200$ ms.

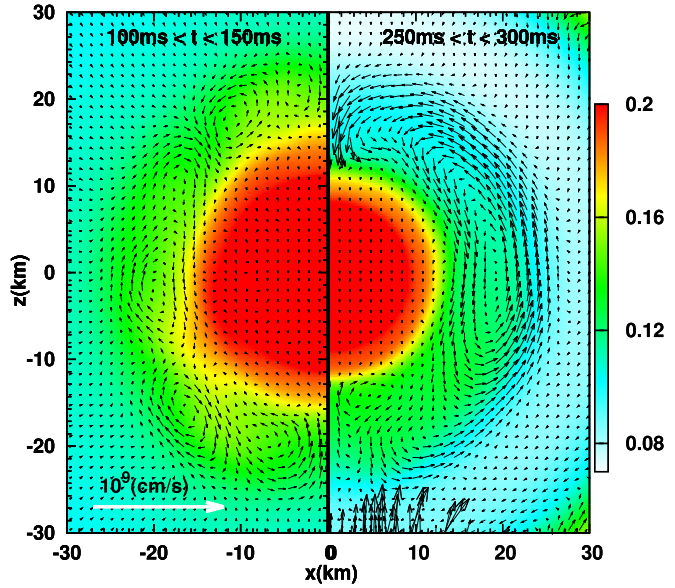

Figure 5. Time average of Y_e in color and fluid velocities as vectors. The left and right panels show the results for the averages over 100 ms $< t <$ 150 ms and 250 ms $< t <$ 300 ms, respectively. Note that the spatial scale and color coding are different from those in Figure 4 and the coordinate origin ($(x, z) = (0, 0)$) in this figure is shifted to the mass center of PNS. See the text for more details.

the region of $20 \lesssim r \lesssim 25$ km at $T_{\rm b} = 200$ ms, which can be understood from a comparison between the vector fields in the left and right panels in Figure 4. At $r \sim 25$ km[9] the fluid velocity (displayed in the left panel) and the $\nu_{\rm e}$ energy flux (displayed on the right panel) deviate from each other.

On the other hand, it is not so easy to identify the cause of the asymmetry in the ν_x luminosity, as the asymmetry is subtle. It may be attributed to the fact that the mass accretion in the northern hemisphere is smaller than in the southern hemisphere, which is caused by the asymmetric shock expansion. As discussed in Nagakura et al. (2019a), the weaker mass accretion facilitates the ν_x diffusion from PNS, and may be responsible for the higher ν_x luminosity in the northern hemisphere. It has been noted that the non-spherical mass accretion may also contribute to the asymmetries in $\nu_{\rm e}$ and $\bar{\nu}_{\rm e}$ luminosities. The effect, however, seems to be minor compared with the contribution from the asymmetric Y_e distribution in the PNS envelope (see below), as the former asymmetry is subtler than the latter.

The asymmetries in $\nu_{\rm e}$ and $\bar{\nu}_{\rm e}$ luminosities reach $\sim$10%. We find that the linear momentum transfer from $\bar{\nu}_{\rm e}$ to matter is slightly larger than that from $\nu_{\rm e}$, which induces the PNS acceleration in the opposite direction to the stronger shock expansion. The asymmetric ν_x emission also enhances the acceleration of PNS.

Note that the sense of the correlation between the asymmetries in $\nu_{\rm e}$ and $\bar{\nu}_{\rm e}$ emissions and that in the shock expansion is the same as in LESA. However, there is no clear indication of deflected accretion streams in the post-shock flow, which were originally suggested as a possible cause of LESA by Tamborra et al. (2014). Instead, the asymmetry of the Y_e distribution is sustained by a long-lived coherent lateral circular fluid motion in the envelope of PNS. In fact, such a coherent motion emerges soon after the asymmetric shock expansion occurs. It is indeed recognized at $10 \lesssim r \lesssim 25$ km between the equator and the north pole (see the vector field of fluid velocity displayed in the left panel of Figure 5).

This is a bit obscured, however, by short-term variations possibly caused by the PNS convection. To see the coherent lateral motion more clearly, we take time-averages of Y_e and fluid velocity for the interval, $250 < t < 300$ ms, the results of which are shown in the right panel of Figure 5. Note that in taking the average we adopt the PNS frame; i.e., the coordinate origin is shifted to the mass center of PNS. For comparison, we also calculate the average over the interval, $100 < t < 150$ ms, and display it in the left panel.

The PNS convection has started before 100 ms; in fact, several eddies can be recognized in the left panel. On the other hand, a large-scale fluid motion is clearly seen in the right panel, which is circulating counter-clockwise in the envelope of PNS at $15 \lesssim r \lesssim 25$ km; it is particularly strong in the northern hemisphere, and there is a small region near the south pole, in which there is a small eddy circulating in the opposite sense. Such large-scale coherent circular motion may not be driven by the PNS convection alone, as the lateral size exceeds the radial width of the convectively unstable region. We argue that this circular motion is triggered by the breaking of up-down symmetry owing to the PNS proper motion and is sustained by the combination of neutrino diffusion, asymmetric matter pressure, and PNS convection. Below we describe this mechanism in more detail.

Once the PNS core ($r < 10$ km) moves downward, the matter distribution in the envelope of PNS starts to adjust itself, inducing a downflow near the north pole and a shear flow between the core and envelope of the PNS in the equatorial region. One may think that the velocity of these down- and shear-flows induced by the PNS proper motion should be of the same order as the velocity of the PNS proper motion ($\sim 10^6$ cm s^{-1}). However, the velocity of the circular motion observed in the simulation is $\sim 10^8$ cm s^{-1}. This may seem to indicate that the self-adjustment of the matter distribution in the PNS envelope cannot be the origin of the circular motion.

This is not true, though. The most important role of the PNS proper motion is to break the up-down symmetry of the matter distribution around the PNS. On the north (south) side, the southward PNS core motion expands (compresses) the PNS envelope. This then extends the low-Y_e region downward in the envelope of PNS on the north side, but shrinks it on the opposite side. This asymmetry in the Y_e distribution triggers the lateral diffusion of neutrinos. Due to the Fermi degeneracy of ν_e, the diffusions of $\nu_{\rm e}$ and $\bar{\nu}_{\rm e}$ occur in the opposite directions (see also Nagakura et al. 2018): $\nu_{\rm e}$ diffuses from higher- to lower-Y_e regions (i.e., from south to north) and $\bar{\nu}_{\rm e}$ does so in the opposite direction. Because neutrino diffusions are accompanied by momentum transfer to matter, they may account for the lateral circular motion.

We estimate the acceleration by the momentum feedback from neutrino to matter and matter-pressure gradient as

$$\bar{a}_{\theta(i)}(r) \equiv -\left\langle \frac{\frac{\partial}{\partial\theta}\bar{P}_i(r,\,\theta)}{r\bar{\rho}(r,\,\theta)} \right\rangle \sim -\frac{\left(\bar{P}_i\left(r,\,\theta=\frac{3\pi}{4}\right) - \bar{P}_i\left(r,\,\theta=\frac{\pi}{4}\right)\right)}{(0.5\pi) r \bar{\rho}_{\rm ave}(r)}, \quad (3)$$

where the symbol – denotes the bar on top of P in Equation (3), and the symbol $\langle\,\rangle$ denotes the time and lateral averages,

[9] The matter density is $\sim 7 \times 10^{12}$ g cm^{-3} at this radius.

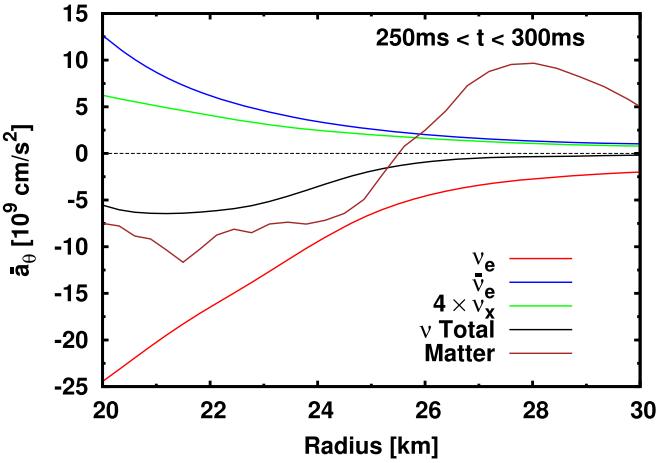

Figure 6. Radial distributions of accelerations induced by the lateral diffusions of different species of neutrinos and matter pressure. The time average is taken over the interval of 250 ms $< t <$ 300 ms (see Equation (3) for the definition).

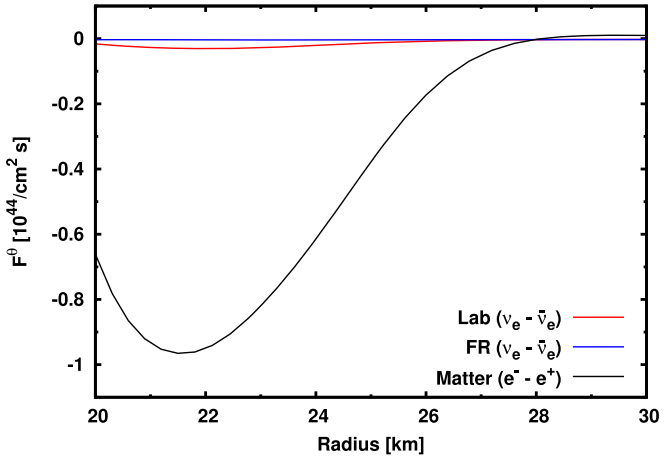

Figure 7. Radial distributions of angle-average lateral number flux of $\nu_e - \bar{\nu}_e$ measured in the laboratory frame (red) and fluid rest frame (blue). The counter part of electron/positron gas corresponds to the black line in the panel.

respectively; the subscript "$i = (\nu, m)$" specifies the neutrino or matter contribution; P_ν stands for the neutrino-pressure, which is approximately evaluated as $E_\nu/3$ in the diffusion regime, and P_m denotes the matter pressure; $\rho_{\rm ave}$ is the angular average of baryon mass density. In Figure 6, we show their radial distributions for the time interval, 250 ms $< t <$ 300 ms.

As can be seen in the figure, ν_e dominates the acceleration and pushes the matter upward, as expected. We also find that the matter-pressure gradient contributes to the lateral acceleration on the same level. It is mainly driven by Y_e asymmetry: the electron/positron pressure is higher in the southern hemisphere, where Y_e is larger and the matter is accelerated upward (but see below for more quantitative arguments). As displayed in Figure 5, the total acceleration is strong at $20 < r < 25$ km, which coincides with the region where we see the fastest fluid motion from south to north (see the right panel of the same figure). As the flow is confined in a closed region, a counter-flow occurs deeper ($15 \lesssim r \lesssim 20$ km) in the PNS envelope (see also the discussions below). The matter velocity (v^θ) produced by the neutrino diffusion and matter-pressure gradient can be estimated more quantitatively as

$$v^\theta \sim (2\bar{a}_\theta L)^{0.5}$$
$$\sim 2\times 10^8 ({\rm cm\ s^{-1}}) \left(\frac{\bar{a}_\theta}{10^{10}\ {\rm cm\ s^{-2}}}\right)^{0.5} \left(\frac{L}{20\ {\rm km}}\right)^{0.5}, \quad (4)$$

where L is the spatial scale of the lateral motion. This is indeed consistent with the velocity observed in the simulation. We thus conclude that both the neutrino diffusion and asymmetric matter-pressure gradient play a major role in the generation of the lateral circular motion.

To see the lateral transport of the lepton number more in detail, we display the radial distributions of angle-averaged lateral lepton number fluxes carried by neutrinos ($F^\theta_{\nu_e} - F^\theta_{\bar{\nu}_e}$, where F^θ denotes the lateral number flux of neutrinos) and by electron/positron in Figure 7. As shown there, the latter is the main contributor to the lepton number transport; indeed, the neutrino contribution is just a few percent. This is simply because the number density of electron/positron is much larger than that for the neutrinos. The neutrino diffusion in the fluid rest frame is even subtler, although it does exist (see the blue line in Figure 7). It should be noted, however, that the momentum feedback from neutrinos is still comparable to the momentum imparted by the matter-pressure gradient, as discussed above. This occurs because the lateral matter-pressure gradient is partially compensated by the temperature asymmetry: the temperature in the northern hemisphere is $\sim$1% higher than in the southern hemisphere. Although the temperature asymmetry is much smaller than that of Y_e, it still reduces the total asymmetry in the matter pressure substantially, because the baryon and photon pressure are dominant in the total pressure.

It is also important to note that Y_e decreases via deleptonization as the matter moves toward the north pole. The Y_e-depleted matter then submerges in the PNS envelope near the north pole. When it hits the PNS core, it is deflected and flows southward along the surface of the PNS core, increasing Y_e this time by ν_e absorptions. The matter emerges again to the PNS surface by the local PNS convection near the south pole. Although the strong downflow induced by the dislocation of PNS tends to suppress the convection around the north pole, the convection activity continues to occur in the vicinity of the south pole and supplies the Y_e-rich material to the PNS envelope there. This closes the cycle and creates the coherent lateral circular motion, with the Y_e asymmetry sustained. Then the circulation will continue until the PNS convection shuts off or the neutrinos in PNS have dried up, both of which may take more than a few seconds. If this is in fact the case, the PNS may be accelerated to more than a hundred km s^{-1}, which is the typical proper motion velocity of pulsars.

Finally, we give some comments on other works on the asymmetric Y_e distributions. Glas et al. (2018) found a circular motion in the envelope of PNS in their 3D simulations, which produced the LESA phenomenon. They speculated that the thermal instability of spherical shells discussed by Chandrasekhar (1961) may be responsible for the sustained asymmetric Y_e distribution. It seems, however, that the circular motion found in their study was not as coherent as what we observed in our study; indeed, they look more like a superposition of some smaller eddies instead (see Figure 6 in Glas et al. 2018). Powell & Müller (2018) also observed LESA in their simulations and suggested that LESA is in effect a manifestation of PNS convections under a different guise. It should be noted that they did not find any coherent circular motions in the envelope of

PNS. Importantly, both simulations sphericalized the matter distribution inside PNS by hand and may have artificially suppressed the proper motion of PNS, which we think is the trigger of the coherent circular motion by breaking the up-down symmetry of the matter distribution around PNS.

5. Summary and Discussion

For decades, asymmetric neutrino emissions have been regarded as a minor player in the generation of NS kick unless some extreme conditions or unknown physics are considered. In our CCSN simulation, however, we find $\sim$10% levels of asymmetry in the energy flux for ν_e and $\bar{\nu}_e$, and $\sim$1% asymmetry for ν_x. The emergence of the coherent asymmetric configurations coincides with the onset of the non-spherical shock expansion and they are sustained at least up to the end of the simulation. Interestingly, they play a non-negligible role in the acceleration of PNSs. The asymmetry of ν_e and $\bar{\nu}_e$ is attributed to that of the Y_e distribution in the envelope of a PNS ($10 \lesssim r \lesssim 25$ km). The self-adjustment of the matter distribution accompanied by the neutrino diffusion there generates a sustained lateral circulation, which in turn works to maintain the asymmetry in the Y_e distribution. It is important to emphasize that all of these dynamics can be captured only with the consistent treatment of neutrino transport and PNS proper motions. Incidentally, Tamborra et al. (2014) and Janka (2017) speculated that LESA may also contribute to the NS kick, but did not demonstrate them quantitatively in their works.

Finally, we present several remarks. As is well known, the imposed axisymmetry artificially enhances the directionality in fluid dynamics such as shock expansions and PNS proper motions. The acceleration of PNSs may hence be overestimated in this study. Nevertheless, the property of asymmetric neutrino emissions ($\bar{\nu}_e$ and ν_x emissions are enhanced in the hemisphere of stronger shock expansion, while ν_e emissions are higher in the opposite hemisphere into which the PNS is accelerated) will remain in 3D; however, this needs to be confirmed in a future study. A longer simulation is definitely required in order to assess how the PNS proper motion found in this Letter affects the hydrodynamic process that occurs later on and is supposed to be the most promising mechanism for the NS kick. It should be emphasized that they are operational in different phases. For example, the current simulation is way too short to see the PNS acceleration by the gravitational tugboat mechanism (Wongwathanarat et al. 2013; Janka 2017). Regardless, what is important is that in some (but not all) cases, the PNS may start to move much earlier than previously thought. Last but not least, the asymmetry in neutrino emissions will affect the collective neutrino oscillation (H. Nagakura et al. 2019, in preparation) and the nucleosynthesis (Fujimoto & Nagakura 2019), both of which are currently being investigated in more details and will be published elsewhere.

We acknowledge Adam Burrows, David Radice, and David Vartanyan for fruitful discussion. The numerical computations were performed on the supercomputers at K, at AICS, FX10 at Information Technology Center of Nagoya University. Large-scale storage of numerical data is supported by JLDG constructed over SINET4 of NII. H.N. was supported by Princeton University through DOE SciDAC4 grant DE-SC0018297 (subaward 00009650). This work was also supported by Grant-in-Aid for the Scientific Research from the Ministry of Education, Culture, Sports, Science and Technology (MEXT), Japan (15K05093, 25870099, 26104006, 16H03986, 17H06357, 17H06365), HPCI Strategic Program of Japanese MEXT and K computer at the RIKEN (Project ID: hpci 160071, 160211, 170230, 170031, 170304, hp180179, hp180111, hp180239).

ORCID iDs

Hiroki Nagakura https://orcid.org/0000-0002-7205-6367
Kohsuke Sumiyoshi https://orcid.org/0000-0002-9224-9449
Shoichi Yamada https://orcid.org/0000-0002-2166-5605

References

Arzoumanian, Z., Chernoff, D. F., & Cordes, J. M. 2002, ApJ, 568, 289
Bisnovatyi-Kogan, G. S. 1993, A&AT, 3, 287
Buras, R., Janka, H.-T., Rampp, M., & Kifonidis, K. 2006, A&A, 457, 281
Chandrasekhar, S. 1961, Hydrodynamic and Hydromagnetic Stability
Chatterjee, S., Vlemmings, W. H. T., Brisken, W. F., et al. 2005, ApJL, 630, L61
Faucher-Giguère, C.-A., & Kaspi, V. M. 2006, ApJ, 643, 332
Foglizzo, T., Kazeroni, R., Guilet, J., et al. 2015, PASA, 32, e009
Fujimoto, S.-i., & Nagakura, H. 2019, arXiv:1906.09553
Fuller, G. M., Kusenko, A., Mocioiu, I., & Pascoli, S. 2003, PhRvD, 68, 103002
Furusawa, S., Togashi, H., Nagakura, H., et al. 2017, JPhG, 44, 094001
Gessner, A., & Janka, H.-T. 2018, ApJ, 865, 61
Glas, R., Janka, H. T., Melson, T., Stockinger, G., & Just, O. 2018, arXiv:1809.10150
Hobbs, G., Lorimer, D. R., Lyne, A. G., & Kramer, M. 2005, MNRAS, 360, 974
Holland-Ashford, T., Lopez, L. A., & Auchettl, K. 2019, arXiv:1904.06357
Holland-Ashford, T., Lopez, L. A., Auchettl, K., Temim, T., & Ramirez-Ruiz, E. 2017, ApJ, 844, 84
Janka, H.-T. 2017, ApJ, 837, 84
Janka, H. T., Melson, T., & Summa, A. 2016, ARNPS, 66, 341
Katsuda, S., Morii, M., Janka, H.-T., et al. 2018, ApJ, 856, 18
Kusenko, A., Mandal, B. P., & Mukherjee, A. 2008, PhRvD, 77, 123009
Lai, D. 2001, LNP, 578, 424
Lyne, A. G., & Lorimer, D. R. 1994, Natur, 369, 127
Mirizzi, A., Tamborra, I., Janka, H. T., et al. 2016, NCimR, 39, 1
Müller, B. 2016, PASA, 33, e048
Müller, B., Janka, H.-T., & Marek, A. 2012, ApJ, 756, 84
Müller, B., Tauris, T. M., Heger, A., et al. 2018, arXiv:1811.05483
Nagakura, H., Furusawa, S., Togashi, H., et al. 2019a, ApJS, 240, 38
Nagakura, H., Iwakami, W., Furusawa, S., et al. 2017, ApJS, 229, 42
Nagakura, H., Iwakami, W., Furusawa, S., et al. 2018, ApJ, 854, 136
Nagakura, H., Sumiyoshi, K., & Yamada, S. 2014, ApJS, 214, 16
Nagakura, H., Sumiyoshi, K., & Yamada, S. 2019b, arXiv:1906.10143
Nordhaus, J., Brandt, T. D., Burrows, A., & Almgren, A. 2012, MNRAS, 423, 1805
Nordhaus, J., Brandt, T. D., Burrows, A., Livne, E., & Ott, C. D. 2010, PhRvD, 82, 103016
Pajkos, M. A., Couch, S. M., Pan, K.-C., & O'Connor, E. P. 2019, arXiv:1901.09055
Powell, J., & Müller, B. 2018, arXiv:1812.05738
Richers, S., Nagakura, H., Ott, C. D., et al. 2017, ApJ, 847, 133
Sagert, I., & Schaffner-Bielich, J. 2008, A&A, 489, 281
Scheck, L., Kifonidis, K., Janka, H. T., & Müller, E. 2006, A&A, 457, 963
Scheck, L., Plewa, T., Janka, H. T., Kifonidis, K., & Müller, E. 2004, PhRvL, 92, 011103
Takiwaki, T., Kotake, K., & Suwa, Y. 2014, ApJ, 786, 83
Tamborra, I., Hanke, F., Janka, H.-T., et al. 2014, ApJ, 792, 96
Togashi, H., & Takano, M. 2013, NuPhA, 902, 53
Winkler, P. F., & Petre, R. 2007, ApJ, 670, 635
Wongwathanarat, A., Janka, H.-T., & Müller, E. 2013, A&A, 552, A126
Woosley, S. E., Heger, A., & Weaver, T. A. 2002, RvMP, 74, 1015